Surface response of a fractional order viscoelastic halfspace to surface and subsurface sources

F. Can Meral and Thomas J. Royston[a)]
Mechanical and Industrial Engineering, University of Illinois at Chicago, Chicago, Illinois 60607

Richard L. Magin
Bioengineering, University of Illinois at Chicago, Chicago, Illinois 60607

(Received 12 June 2009; revised 3 September 2009; accepted 6 September 2009)

Previous studies by the second author published in this journal focused on low audible frequency (40–400 Hz) shear and surface wave motion in and on a viscoelastic material representative of biological tissue. Specific cases considered were that of surface wave motion on a halfspace caused by a finite rigid circular disk located on the surface and oscillating normal to it [Royston *et al.*, J. Acoust. Soc. Am. **106**, 3678–3686 (1999)] and compression, shear, and surface wave motion in a halfspace generated by a subsurface finite dipole [Royston *et al.*, J. Acoust. Soc. Am. **113**, 1109–1121 (2003)]. In both studies, a Voigt model of viscoelasticity was assumed in the theoretical treatment, which resulted in agreement between theoretical predictions and experimental measurements over a limited frequency range. In the present article, the linear viscoelastic assumption in these two prior works is revisited to consider a (still linear) fractional order Voigt model, where the rate-dependent damping component that is dependent on the first derivative of time is replaced with a component that is dependent on a fractional derivative of time. It is shown that in both excitation source configurations, the fractional order Voigt model assumption improves the match of theory to experiment over a wider frequency range (in some cases up to the measured range of 700 Hz). © *2009 Acoustical Society of America.* [DOI: 10.1121/1.3242351]

PACS number(s): 43.80.Cs, 43.80.Ev, 43.20.Jr [FD] Pages: 3278–3285

I. INTRODUCTION

An improved understanding of mechanical wave propagation in viscoelastic materials and structures could fundamentally catalyze technical developments in many areas including medicine, geophysics, infrastructure, and manufacturing. For example, it could lead to improved medical imaging[1] (e.g., dynamic elastography), improved land mine,[2] and other buried object detection,[3] earthquake and tsunami monitoring and analysis,[4–6] intelligent bridge and civil structure assessment,[7] and improved nondestructive testing of man-made materials and components,[8,9] at microscopic and macroscopic scales. In medical imaging, in particular, noninvasive measurement of shear wave motion in soft biological tissues can provide unique spatially localized information about the tissue's material properties. Such information can reflect the development of pathology and in some cases biomechanical integrity. Additionally, it may provide a unique way to nondestructively track the morphogenesis of engineered tissues. Over the past few decades, mechanical wave propagation has been combined with the medical imaging modalities of ultrasound or magnetic resonance (MR) imaging to establish noninvasive means of visualizing shear wave motion for diagnosis or nondestructive tissue assessment.[10–14] These dynamic elastography imaging techniques, as they are commonly referred, have received much attention because shear moduli have a large dynamic range within soft biological tissues, particularly when compared with the variation in material parameters that provide contrast in conventional imaging techniques. For soft biological tissues (e.g., comparing muscle with fat), the x-ray attenuation coefficient varies only by a factor of 2,[15] while MR relaxation times vary by a factor of 3.[16] The shear moduli, on the other hand, can vary by more than a factor of 10.[17–19]

Estimating material properties based on dynamic elastography images is called inversion or reconstruction. Different techniques have been proposed including, for example, "local frequency estimation,"[20] "algebraic inversion of the differential equation,"[21] other "variational" methods,[22,23] and "finite element model reference" based methods[24,25] to name a few. Additionally, focused modulated radiation force of ultrasound at multiple frequencies has been used to remotely drive an embedded hard target[26] and to generate shear waves[27,28] in order to estimate the medium's viscoelastic properties based on measurements of the target's motion or the speed of shear wave propagation as a function of frequency. These techniques often assume a constitutive relation for the tissue viscoelasticity, such as a Voigt model, to aid in interpreting measurements. Studies have shown that such viscoelastic models have limitations in their ability to accurately model dynamic phenomena over multiple time scales and/or with broad spectral content, particularly for biological tissues and tissue mimicking phantoms, and that one way of overcoming such limitations is through the use of fractional order models.[29–33] Fractional order viscoelastic modeling starts with the idea from fractional calculus that the order of the derivative of the strain can be intermediate between 0 and 1 since it is the derivative of the strain that characterizes the material's behavior (assuming a one dimensional stress-strain relation). Such an approach offers a new

a)Author to whom correspondence should be addressed. Electronic mail: troyston@uic.edu

viscoelastic stress-strain model. When the order of the derivative is zero, it represents a Hookean solid and when it is of order 1, it describes a Newtonian fluid. Viscoelastic materials occupy the intermediate range with a fractional order "α" between 0 and 1. Using this approach, it is possible to build a multi-component fractional equivalent of the "standard linear solid" (SLS) by replacing one or more springs and dashpots with "springpots." Such models are linear and have shown the potential to yield new disease and treatment specific parameters that more effectively predict underlying changes in tissue associated with developing pathology, such as liver cirrhosis and breast cancer. As an example, in Ref. 33 a relatively simple power law relationship was fitted to the complex shear modulus of human breast tissue and tumors measured by magnetic resonance elastography. The results, when plotted as the fractional power exponent versus the fractional order attenuation, separated benign from malignant tumors with an increase in specificity and sensitivity.

In previous studies by the second author of the present article[34,35] there has been an emphasis on understanding the shear wave field created in a material like biological tissue by canonical vibratory sources. In Ref. 34, a new analytical solution was derived for the problem of surface wave generation on a linear viscoelastic halfspace caused by a finite rigid circular disk located on the surface and oscillating normal to it. While the motivation of the work was to better understand surface wave propagation in biological tissue, the solution approach taken was an incremental advancement of theoretical work reported in seminal articles in the geophysics literature.[5,6] The improved solution was tested experimentally using a viscoelastic phantom with material properties comparable to biological soft tissue. Some agreement could be achieved over a limited frequency range (20–100 Hz) using a Voigt model. Another study[35] analyzed compression, shear, and surface waves in a viscoelastic halfspace generated by subsurface fundamental acoustic sources. Finite and infinitesimal monopole and dipole sources within the low audible frequency range (40–400 Hz) were considered theoretically, computationally and, in some cases, experimentally for a soft tissue phantom material. Again, a Voigt model was assumed, which produced results that matched experiment over a limited frequency band.

In the present article, in order to improve material characterization over a broader frequency range, we revisit the viscoelastic modeling assumption in these two prior works[34,35] to consider fractional order components. Specifically, our objectives are to reconsider wave motion on the surface of a viscoelastic medium (halfspace) created by finite dimension surface and subsurface vibratory sources oscillating normal to the planar surface of the medium. Theoretical predictions for the case of a material with fractional viscoelastic properties are derived and compared with experimental studies. Their ability to match experimental measurements is compared with the conventional (integer order) Voigt and standard linear solid (also known as Kelvin or Zener) models.

II. FRACTIONAL VISCOELASTIC CONTINUUM: GOVERNING EQUATIONS

For an isotropic, homogenous, viscoelastic compressible medium, one can use the following formulation of the equation of motion for small perturbations about an operating point

$$(\lambda + \mu)\,\nabla\nabla\cdot\mathbf{u} + \mu\nabla^2\mathbf{u} = \rho\frac{\partial^2\mathbf{u}}{\partial t^2}. \tag{1}$$

Here, $\mathbf{u}$ is the displacement vector, ρ is the density of the medium, $\partial/\partial t$ denotes a derivative with respect to time, ∇ is the spatial Laplacian operator dependent on the chosen coordinate system, and λ and μ are the Lamé constants of the medium. For a linear viscoelastic Voigt material model, the rate-dependent Lamé "constants" are expressible as $\lambda(t) = \lambda_0 + \lambda_1\partial/\partial t$ and $\mu(t) = \mu_0 + \mu_1\partial/\partial t$, where λ_0, λ_1, μ_0, and μ_1 are coefficients of volume compressibility, volume viscosity, shear elasticity, and shear viscosity, respectively.[36] Other shear viscoelastic models will lead to different rate-dependence relations.

With regard to μ, it has been observed in many materials that the simple two-element Voigt model for shear viscoelasticity (μ_0, μ_1) does not accurately capture material shear dynamic behavior, in terms of its experimentally measured response to various elementary excitation waveforms, such as step inputs or periodic or random inputs with broad spectral content. More complex arrangements of multiple elastic (springs) and viscous (dashpot) components may then be employed empirically in order to more closely match what is observed. For example, the SLS model, also known as the Kelvin or Zener model, consists of a parallel combination of a Maxwell element (spring and dashpot in series) with a spring. The three-element SLS model has more flexibility in representing dynamic viscoelasticity as compared to the Voigt model.[18] Instead of increasing the constitutive model complexity by increasing the number of components that comprise it, an alternative is to consider that the material may exhibit rate-dependent shear deformation that is best described by a single element, comprised of two constants, μ_α and α, whose behavior lies somewhere between Hookean solid and Newtonian fluid. Specifically, fractional order viscoelasticity (a springpot) can be specified as shown in the second term of the following:

$$\mu = \mu_0 + \mu_\alpha\frac{\partial^\alpha}{\partial t^\alpha}, \quad 0 < \alpha \leq 1. \tag{2}$$

Henceforth, Eq. (2) will be referred to as a fractional order Voigt model for $\alpha < 1$. While such a mathematical construction may seem to lack physical meaning, it can be shown that this type of relation results asymptotically when using a ladder-like fractal arrangement of integer-order elastic and viscous components, as depicted in Fig. 1.[37] Indeed, such an arrangement might be rationalized on the grounds that it represents multiscale rate-dependent stress-strain interactions that one would inherently expect in some materials with complex multiscale cellular and extracellular structure, such as biological tissues. Furthermore, suitably defined fractional derivatives do not pose significant difficulty mathematically

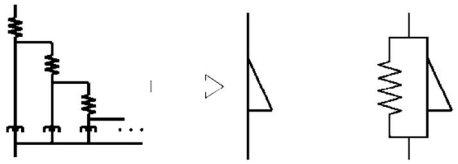

FIG. 1. A tree arrangement of springs and dashpots (left) resulting in a fractional order element, called a springpot (middle). Schematic representation of a fractional order Voigt model (right); the dashpot is replaced with a springpot.

for well-conditioned functions. [In this paper, we have chosen to use the Weyl definition of the fractional order derivative, which for harmonic functions such as $f(t)=e^{j\omega t}$, has the property that $\partial^\alpha/\partial t^\alpha[e^{j\omega t}]=(j\omega)^\alpha e^{j\omega t}$.] The expression in Eq. (2) is still linear in nature and thus all rules and techniques afforded such relations, such as the validity of superposition, reciprocity, the Laplace and Fourier transforms, with associated transfer and frequency response functions, are all still valid.[37] In the Laplace (s) and frequency ($j\omega$) domains where $j=\sqrt{-1}$ and ω is the circular frequency, Eq. (2), respectively, becomes

$$\mu = \mu_0 + \mu_\alpha (s)^\alpha, \tag{3a}$$

$$\mu = \mu_0 + \mu_\alpha (j\omega)^\alpha. \tag{3b}$$

Note that a significant attribute of such fractional representations is that the temporal response takes on characteristics of power-law behavior as opposed to the exponential response that one obtains with the conventional Voigt representation. A power-law response, in fact, has been observed in a number of biological and nonbiological materials, further motivating this type of model.[30,31]

Regardless of whether an "integer order" or fractional order Voigt model or a standard linear solid model is used, wave motion in the *infinite* three-dimensional viscoelastic medium consists of a superposition of dilatational and shear wave displacements, $\mathbf{u}=\mathbf{u_P}+\mathbf{u_S}$, respectively. For the *semi-infinite* halfspace problem, an additional surface (Rayleigh) wave $\mathbf{u_{Su}}$ will exist for the configurations considered in Sec. III.

III. SURFACE WAVE PROPAGATION ON A HALFSPACE DUE TO A SURFACE SOURCE

A. Theory

In Ref. 34, a simplified analytical solution is derived for Rayleigh wave propagation on the surface of an isotropic homogeneous viscoelastic halfspace caused by normal force excitation over a circular region of radius a on the surface of amplitude per unit area P_{in} with harmonic time dependence $e^{j\omega t}$ as depicted in Fig. 2. The analytical solution is

$$\frac{u_z}{P_{\text{in}}} = -\frac{2a}{\mu}\frac{J_1(pak_p)\sqrt{p^2-1}}{F_0'(-p)}\eta^2 K_0(jprk_p)e^{j\omega t}, \tag{4a}$$

where

$$F_0'(-p) = \left.\frac{\partial F_0}{\partial \zeta}\right|_{\zeta=-p}, \tag{4b}$$

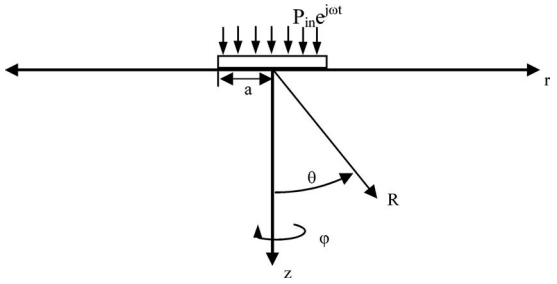

FIG. 2. Ideal viscoelastic halfspace with finite surface source.

$$F_0(\zeta) = (2\zeta^2-\eta^2)^2 - 4\zeta^2\sqrt{\zeta^2-\eta^2}\sqrt{\zeta^2-1}, \tag{4c}$$

$$\eta = \sqrt{(\lambda+2\mu)/\mu}, \tag{4d}$$

$$k_p = \omega\sqrt{\rho/(\lambda+2\mu)}. \tag{4e}$$

Here, u_z is out-of-plane surface displacement, p is the ratio of compression wave speed to surface wave speed and is a root of the function F_0 that is associated with Rayleigh wave motion, k_p is the compression wave number, r is the radial distance from center of the driving disk, J_1 is the Bessel function of the first kind (order 1), and K_0 is the modified Bessel function of the second kind (order 0); K_0 can also be written in terms of Bessel functions of the first and second kinds (order 0) such as $K_0(x)=(\pi/2)i\{J_0(ix)+iY_0(ix)\}$. Equation (4c) links compression, shear, and surface wave behaviors to material viscoelastic properties; the roots of this equation yield compression, shear, and surface wave numbers.

Shear wave speed velocity at frequency ω is related to the real (storage) and imaginary (loss) parts of the shear modulus, μ_R and μ_I respectively, and the material density ρ as[14]

$$c_s = \sqrt{\frac{2}{\rho}\frac{\mu_R^2+\mu_I^2}{\mu_R+\sqrt{\mu_R^2+\mu_I^2}}}. \tag{5}$$

If surface wave speed and attenuation are experimentally measured, material properties that affect shear and surface wave speed can be estimated using Eqs. (4a)–(4e) and (5). Note that both μ_R and μ_I are independent of whether the time derivative part of the Voigt model is of integer or fractional order. They are equal to μ_0 and $\omega\mu_1$, shear elasticity and shear viscosity multiplied with circular frequency, if a conventional integer order Voigt model is used. In the case of a fractional order Voigt model since $(j\omega)^\alpha=\omega^\alpha(\cos[\alpha\pi/2]+j\sin[\alpha\pi/2])$, the storage modulus and loss modulus are defined, respectively, as

$$\mu_R = \mu_0 + \mu_\alpha\omega^\alpha\cos\left(\frac{\pi}{2}\alpha\right), \tag{6a}$$

$$\mu_I = \mu_\alpha\omega^\alpha\sin\left(\frac{\pi}{2}\alpha\right). \tag{6b}$$

Alternatively, the SLS model yields

$$\mu_R = \frac{\mu_0\mu_\omega^2+\omega^2\mu_1^2(\mu_0+\mu_\omega)}{\mu_\omega^2+\omega^2\mu_1^2}, \tag{7a}$$

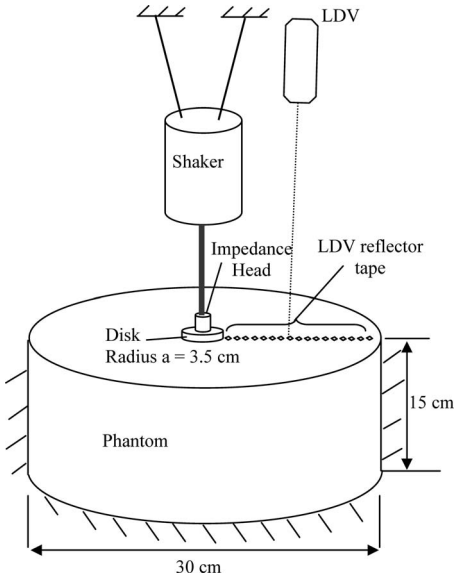

FIG. 3. Experimental schematic for measurement of surface wave motion caused by a surface source using a LDV.

$$\mu_I = \frac{\omega \mu_\omega^2 \mu_1}{\mu_\omega^2 + \omega^2 \mu_1^2}. \tag{7b}$$

Here μ_0 denotes the static stiffness, μ_1 denotes the viscous damping coefficient multiplied with the first order time derivative of the displacement (thus α is equal to 1), and μ_ω denotes the dynamic stiffness, which is only effective when the loading has a non-zero time derivative.

B. Experiment

Surface wave experiments were conducted as depicted in Fig. 3 using a silicone polymer, CF-11 (NuSil Technology, Carpinteria CA), which had a density of 1100 kg/m^3 calculated through basic mass volume measurements of small test specimens. While in liquid form, the material is poured into the container and then cures at room temperature. The container is mounted on a vibration isolated optics bench. A plexiglass disk, driven by a mechanical shaker (ET-132, LabWorks Inc., Mesa Costa, CA) that is supported by a separate structure, is positioned on the surface of the phantom with a sufficient preload to ensure contact during excitation. The shaker is driven via an amplifier (Type 2076, Bruel & Kjaer, Denmark) with a signal input from a dynamic signal analyzer (35670A, Agilent Technologies, Santa Clara, CA). The force and acceleration of the disk are measured with an impedance head (288D01, PCB Piezotronics, Depew, NY), and the out-of-plane velocity at discrete points on the surface is measured using a laser Doppler vibrometer (LDV) (CLV-800, Polytec, Tustin, CA). Small ($\sim$2 mm^2) pieces of 3M retroreflective tape are mounted on the semi-translucent phantom material to aid in LDV measurement. Measurement signals are recorded and the frequency response function (FRF) between the output (vertical velocity of the surface points) and input (motion input of the disk) is calculated by the dynamic signal analyzer. Further analysis of the data is conducted in MATLAB® (Mathworks, Natick, MA).

Additionally, a static measurement of the phantom material stiffness was made by indenting a steel sphere of diameter 9.525 mm into the media. Indentation forces were measured for different indentation depths using a force gauge (Model DPS, Imada, Northbrook, IL). Indentation of the steel ball into the semi-infinite medium was assumed to be a Hertzian contact problem and the solution given by Timoshenko[38] was used:

$$a = \sqrt[3]{\frac{9\pi^2}{16} \frac{P^2 (k_1 + k_2)^2 (R_1 + R_2)}{R_1 R_2}}, \tag{8}$$

where

$$k_i = \frac{1 - \nu_i^2}{\pi E_i}, \quad i = 1,2. \tag{9}$$

Here, P is the indentation force, E_i and ν_i are Young's modulus and Poisson's ratio, respectively, of the two materials in contact, a is the indentation depth, and R_1 and R_2 are the radii of two spherical bodies; in our case one of the bodies was an infinite halfspace, yielding $R_1 = \infty$. Also the indenter ball was very stiff compared to the medium being indented; $E_2 = \infty$. These assumptions simplify the equation so that Young's modulus of the halfspace could be calculated using

$$E_1 = \sqrt{\frac{9}{16} \frac{P^2 (1 - \nu_1^2)^2}{a^3 R_2}}. \tag{10}$$

Given that the halfspace material is nearly incompressible ($\nu \approx 0.5$), we then have $\mu_0 = E_1/3$.

C. Results and discussion

Due to the finite size of the viscoelastic phantom (it is not an infinite halfspace), resonant behavior is observed at lower frequencies. Also, surface velocity measurement data from points further than 10 cm from the source cannot be used due to the high attenuation and/or reflections from the boundaries. The amplitude and phase information of the complex frequency response data are used to calculate the surface wave speed and rate of attenuation at different frequencies from the remaining points. The real part of the surface wavenumber, pk_p, is obtained from the surface wave phase speed. Based on the term $K_0(jprk_p)$ in Eqs. (4a)–(4e), an estimate of complex value p is then obtained as a function of ω. This is then used with Eqs. (4a)–(4e) to calculate the complex shear wave number, ηk_p. From this, one then can calculate the real and imaginary parts of the complex shear modulus, μ_R and μ_I, respectively, as a function of frequency. Results are shown in Fig. 4.

The conventional Voigt model, SLS model, and the fractional order Voigt model for shear viscoelasticity were used to fit the experimental data. Volume elasticity, λ_0, primarily affects compression wave speed and should not affect shear or surface wave speed. Nonetheless, an approximate value was needed for Eqs. (4a)–(4e). Given that the speed of sound (compression waves) in CF-11 was comparable to water, a value of $\lambda_0 = 2.9$ GPa was used. Volume viscosity, λ_1, is assumed negligible for the low frequencies considered in this study.[36] A value for shear elasticity μ_0, which is common to all three shear viscoelasticity models (Voigt, SLS, fractional

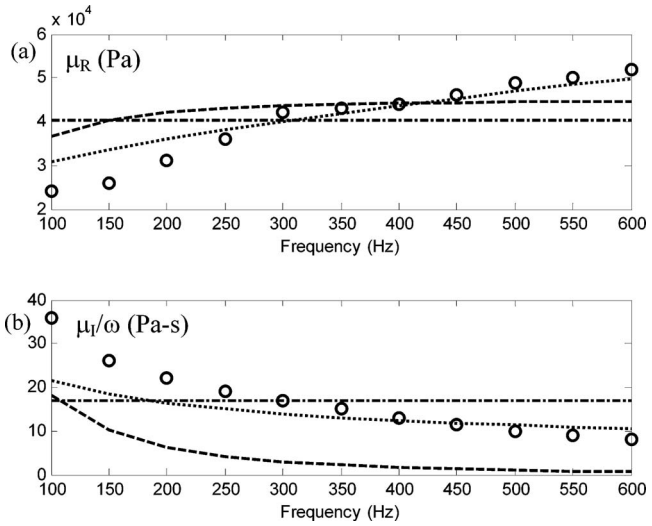

FIG. 4. CF-11 complex shear modulus $\mu=\mu_R+j\mu_I$ as a function of frequency: (a) real part; (b) imaginary part/ω. (○ ○ ○) experimentally derived values; (---) best fit Voigt model; (···) best fit $\alpha=0.6$ fractional order Voigt model; (---) best fit SLS model.

Voigt), was available from the static indentation test described above and is provided in Tables I and II. That value is used in the SLS and fractional order Voigt models, then leaving two parameters in each of those models to be optimized based on the dynamic experimental surface wave data. For the conventional Voigt model, a different value for μ_0 is calculated by determining the average value of the real part of the shear modulus, μ_R, based on the experimental measurements over the frequency range shown in Fig. 4. Similarly, for the conventional Voigt model μ_1 is determined by matching it to the average value of the imaginary part of the shear modulus, μ_I, divided by frequency ω based on the experimental measurements over the frequency range shown in Fig. 4. For the SLS model, note in Eq. (7a) that the value of μ_R approaches $\mu_0+\mu_\omega$ as ω increases; thus, μ_ω was chosen by subtracting μ_0 from the average of μ_R at higher frequencies (>500 Hz). Then, μ_1 was chosen to minimize the least squares error for both μ_R and μ_I based on the experimental measurements over the frequency range shown in Fig. 4. The values of μ_ω and μ_1 yielding the best overall fit are shown in Fig. 4 and in Table I. For the fractional order Voigt model, α was varied in increments of 0.05 between 0 and 1 and μ_α was then chosen to minimize the least squares error for both μ_R and μ_I based on the experimental measurements over the frequency range shown in Fig. 4. The values of α and μ_α yielding the best overall fit are shown in Fig. 4 and in Table I.

TABLE I. CF-11 best fit viscoelastic constants for surface wave experiments for Voigt, fractional order Voigt, and SLS models. (For the fractional order Voigt and SLS models, μ_0 is the value obtained from the static indentation test. For the Voigt model, μ_0 is the average value of real part of complex μ in the frequency range of interest.)

	$\alpha=1$	$\alpha=0.6$	SLS, $\alpha=1$
μ_0 (Pa)	40 300	21 000	21 000
μ_α (Pa s$^\alpha$)	17	351	51
μ_ω (Pa)	···	···	24 000

TABLE II. CF-11 best fit viscoelastic constants for dipole experiments for Voigt, fractional order Voigt, and SLS models. (For the fractional order Voigt and SLS models, μ_0 is the value obtained from the static indentation test. For the Voigt model, μ_0 is the average value of real part of complex μ in the frequency range of interest.)

	$\alpha=1$	$\alpha=0.6$	SLS, $\alpha=1$
μ_0 (Pa)	47 100	21 000	21 000
μ_α (Pa s$^\alpha$)	33.7	553	70
μ_ω (Pa)	···	···	40 000

In Fig. 4, the increasing trend of the storage modulus (μ_R) with frequency is evident; this behavior is not represented by the conventional Voigt model for which $\mu_R=\mu_0$, a constant. The ratio μ_I/ω is also plotted and has a decreasing frequency trend, though for the conventional Voigt model $\mu_I/\omega=\mu_1$ is a constant. While the optimized SLS model does have these frequency-dependent trends in μ_R and μ_I/ω, as shown in Fig. 4, the optimized fractional order Voigt model was better able to track the frequency dependence of both the storage and loss moduli. As noted above, for both SLS and fractional order Voigt models, the value of μ_0 was independently fixed based on the static indentation test, leaving two parameters in each of these models to be optimized based on the dynamic surface wave experimental data. Of course, increasing the number of parameters that can be adjusted in either integer or fractional order models improves the fit to experiment. The point made here is that the fractional order Voigt model, with two parameters, α and μ_α, optimized based on the dynamic data, provides a better fit than the SLS model, with two parameters, μ_1 and μ_ω, optimized based on the same dynamic experimental data.

IV. SURFACE MOTION ON A HALFSPACE DUE TO A SUBSURFACE (DIPOLE) SOURCE

A. Theory

In 1955, Pekeris[39] derived integral expressions for wave motion due to the buried vertical *infinitesimal* dipole (a point force) in a halfspace. With respect to the problem of a *finite* dipole in a semi-infinite viscoelastic or elastic halfspace, as depicted in Fig. 5, we have not found a closed-form analytical solution in the literature. However, an approximate approach is to take the solution for a dipole in an infinite me-

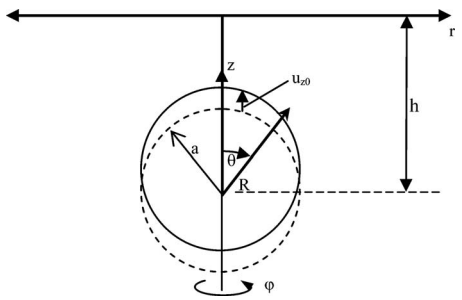

FIG. 5. Ideal viscoelastic halfspace with finite subsurface (dipole) source.

dium and then double its predicted value at the actual location of the free surface. The dipole source produces both dilatational (compression) and shear wave motion; however, in addition to conversions between dilatational and shear wave types, which will occur at the surface, Rayleigh (surface) waves are not accounted for in such an approximation. In prior work of the second author, it was shown that for a material comparable to soft biological tissue, this was an accurate approximation for both infinitesimal and finite dipole sources relatively near the free surface.[35] This approach is adapted here for the finite dipole case, but now with the consideration of the SLS and fractional order Voigt viscoelastic models.

Consider a rigid sphere of radius a embedded in an isotropic viscoelastic medium that is executing rectilinear motion along the z axis given by $u_z = u_{z0}e^{j\omega t}$, as depicted in Fig. 5. This gives rise to dilatational and shear waves in the surrounding medium. Because of axisymmetry, $u_\phi = 0$ and the displacement vector on the sphere surface is $\mathbf{u} = [u_R, 0, u_\theta]^T$, in spherical coordinates where $u_R = u_R(R, \theta, t)$ and $u_\theta = u_\theta(R, \theta, t)$. The resulting displacement fields u_R and u_θ may be expressed as

$$\mu_R = N_1 \cos(\theta)\{[2 + 2jk_pR - (k_pR)^2]e^{-jk_pR} + 2N_2(-jk_sR - 1)e^{-jk_sR}\}e^{j\omega t}/R^3, \quad (11a)$$

$$u_\theta = -N_1 \sin(\theta)\{(-jk_pR - 1)e^{-jk_pR} + N_2[1 + jk_sR - (k_sR)^2]e^{-jk_sR}\}e^{j\omega t}/R^3, \quad (11b)$$

where values for N_1 and N_2 are given in Ref. 35 and are dependent on the assumed boundary condition, welded or slip, at the sphere surface. Here again, while previous studies that have used this equation have assumed a conventional "integer order" Voigt model, a fractional order Voigt model is easily employed.

B. Experiment

An experimental study was conducted for the case of the finite dipole buried in a viscoelastic medium with finite boundaries. The medium is the silicone-based polymeric gel CF-11 described in Sec. III B. A diagram of the experimental apparatus is shown in Fig. 6. A steel sphere is mounted to a mechanical shaker (4808, Bruel & Kjaer, Denmark) via a steel stinger that has a smooth, lubricated surface and via an impedance head (288B02, PCB Piezotronics, Depew, NY). The stinger and sphere are mounted in a container over the shaker via a rubber diaphragm at the base of the container. The silicone material in liquid form is poured into the container until it covers the sphere to the desired depth. The silicone container is mounted on a vibration isolated optics bench. The shaker is mounted on a separate support structure below the bench, with the stinger coming up through a clearance hole drilled in the optics bench below the annular rubber diaphragm at the base of the silicone-filled container. The surface response of the phantom material to shaker driven excitation is measured using a LDV (CLV-800, Polytec, Tustin, CA). Small (~ 2 mm^2) pieces of 3M retro-reflective tape are mounted on the semi-translucent phantom material to aid

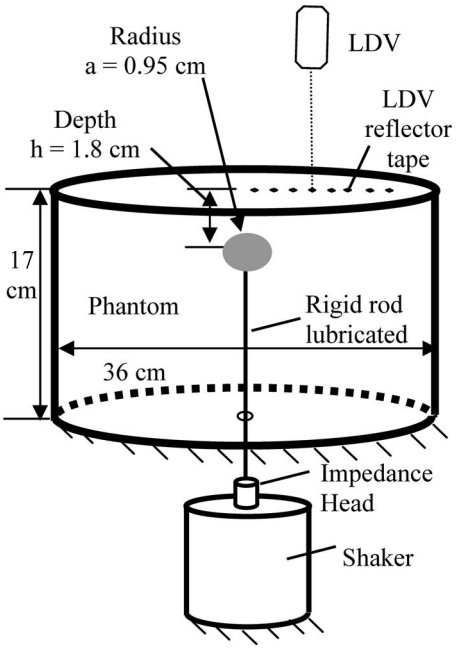

FIG. 6. Experimental schematic for measurement of surface wave motion caused by a subsurface (finite dipole) source.

in LDV measurement. Additionally, the vertical motion of the rigid sphere embedded in the phantom material just below its surface can be measured using the LDV because of the translucent nature of the phantom material. In MATLAB®, the frequency response of the system is calculated, using the rigid sphere velocity as the input and the phantom vertical surface velocity as the output. In theory, this FRF should not be affected by any resonant properties of the rod and sphere connected to the shaker, as these dynamics, present in both the input and output of the FRF, should effectively cancel one another. However, as results show in Sec. III C, a strong resonance of the rod-sphere-shaker system near 200 Hz does seem to alter calculated system values based on this FRF measurement.

C. Results and discussion

Measured and calculated vertical surface motion at four frequencies as a function of radial location is shown in Fig. 7. (These are the same four frequencies used in Ref. 35.) The analytically calculated surface response based on Eq. (11) and the three different viscoelasticity models (integer and fractional order Voigt, and SLS) consists of compression and shear waves, which are also plotted individually to show their relative contribution.

For all three viscoelastic models, at 40 and 80 Hz the shear wave component is dominant and thus its line is nearly indistinguishable from the line for the sum of the compression and shear waves. This is also true for the fractional order Voigt and SLS models at 200 Hz, and only for the SLS model at 400 Hz. The explanation for this is as follows. Both integer and fractional order Voigt models yield a loss modulus μ_I that increases with frequency; for the integer order model, it increases linearly with frequency and for the fractional order model it increases with the α power of frequency where $\alpha < 1$; see Eq. (6b). This increase results in greater

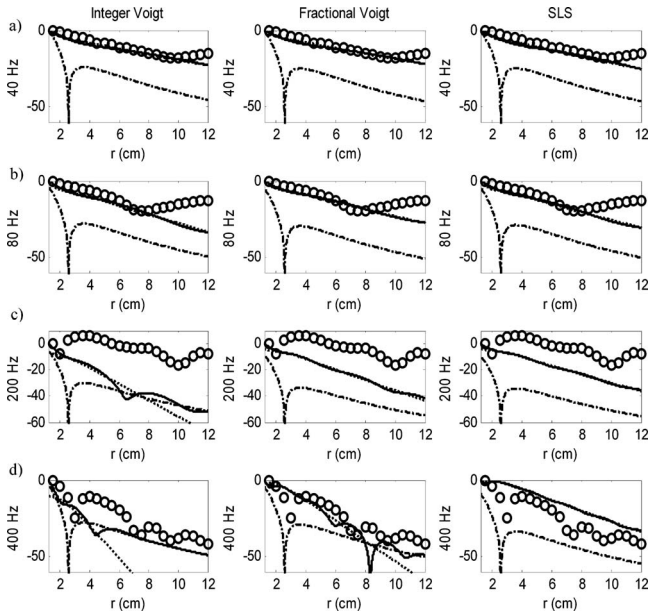

FIG. 7. The surface response of the viscoelastic halfspace to a subsurface (dipole) excitation as a function of radial position r for four different frequencies: (a) 40 Hz, (b) 80 Hz, (c) 200 Hz, and (d) 400 Hz. Columns: (1) Voigt model; (2) Fractional order Voigt model; (3) SLS model. (○○○) experimental measurement; (---) compression wave component; (···) shear wave component; (——) sum of compression and shear waves.

attenuation of shear wave motion as frequency increases, relative to compression waves. Contrary to the Voigt models, for the SLS model the loss modulus μ_I decreases with frequency; see Eq. (7b). Consequently, this model predicts that the shear wave contribution to surface motion will remain larger than the compression wave contribution as frequency increases, as shown in Fig. 7. This is not consistent with experimental studies.

In Fig. 8, the real and imaginary parts of the shear modulus are shown based on the experimental measurements and theoretical models. The measurement-based values were determined at each frequency point by a least squares error

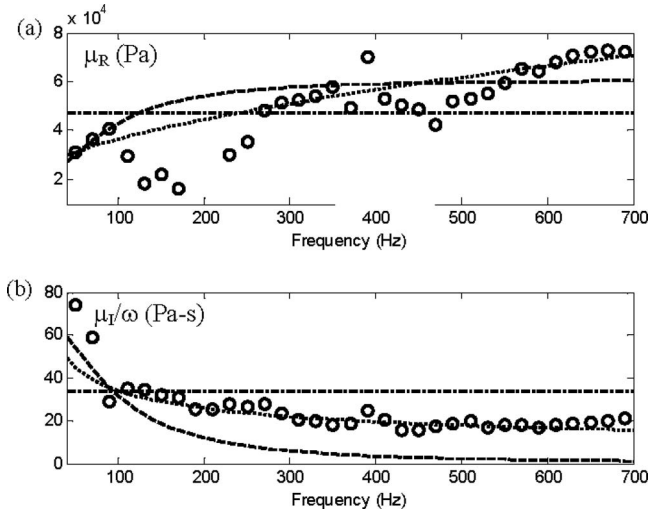

FIG. 8. CF-11 complex shear modulus $\mu=\mu_R+j\mu_I$ as a function of frequency for subsurface (dipole) source study. (a) Real part. (b) Imaginary part/ω. (○○○) experimentally derived values; (---) best fit Voigt model; (···) best fit $\alpha=0.6$ fractional order Voigt model; (---) best fit SLS model.

fit of the measured FRF value at the radial measurement points to the predicted values using Eq. (11), where all other parameters except complex μ are known and given in Sec. III. Once the measurement-based values for μ were determined over the frequency range shown in Fig. 8, least squares error fits of the three viscoelastic models were calculated in the same way as described in Sec. III C. Like before, the statically determined μ_0 was used for the SLS and fractional order Voigt model, leaving two parameters each for these models to be optimized based on the dynamic data. Optimal parameter values for these models are provided in Table II and the real and imaginary parts of the shear modulus based on them are shown in Fig. 8. The analytically calculated surface responses shown in Fig. 7 for the different optimal viscoelastic models could then be determined using Eq. (11).

As noted in Sec. III, the conventional Voigt model assumes constant values μ_R and μ_I/ω. As seen in Fig. 8, experiment-based values for both these parameters change with frequency. The SLS and fractional order Voigt models are able to represent this frequency dependence (though not the variation in the vicinity of 200 Hz, a strong resonance of the dipole source as mentioned in Sec. IV B). At the lower frequencies shown in Fig. 7, 40 and 80 Hz, all three models yield comparable results. However, at the higher frequencies the optimal fractional order Voigt model clearly performs better than the other two, being able to capture some of the unique radially dependent features of the response. Also, note that the optimized values for CF-11 fractional viscoelasticity, in terms of the order α and value of μ_α, are roughly in agreement based on two different types of measurements, surface motion due to a surface source (Sec. III) and due to a subsurface source (this section), given that there is some expected variation between different molds of the material.

V. CONCLUSION

The viscoelastic assumption in two prior studies of surface and shear wave motion on a halfspace has been reconsidered. Studies reported here show that a simple *fractional order* Voigt model, one with a fractional time derivative in its rate-dependent component, significantly improves the match of theory to experiment over a wider frequency range, as compared to the conventional integer order Voigt model and to the standard linear solid model, which has the same number of independent parameters as the fractional order Voigt model. The underlying physical motivation for the use of a fractional viscoelastic assumption and the potential practical benefits, such as improved medical diagnostics, were discussed. Improved model accuracy may be possible by incorporating additional fractional elements; a more thorough investigation of the fundamentals governing viscoelastic behavior at multiple scales in such materials may serve to motivate and direct such an investigation in the future.

ACKNOWLEDGMENTS

The financial support of the National Institutes of Health (Grant Nos. EB004885, EB008373, and EB007537) is acknowledged.

[1]J. F. Greenleaf, M. Fatemi, and M. Insana, "Selected methods for imaging elastic properties of biological tissues," Annu. Rev. Biomed. Eng. **5**, 57–78 (2003).
[2]N. Xiang and J. M. Sabatier, "An experimental study on antipersonnel landmine detection using acoustic-to-seismic coupling," J. Acoust. Soc. Am. **113**, 1333–1341 (2003).
[3]C. H. Frazier, N. Cadalli, D. C. Munson, Jr., and W. D. O'Brien, Jr., "Acoustic imaging of objects buried in soil," J. Acoust. Soc. Am. **108**, 147–156 (2000).
[4]R. A. Sohn and J. A. Hildebrand, "Hydroacoustic earthquake detection in the Artic basin with the Spinnaker array," Bull. Seismol. Soc. Am. **91**, 572–579 (2001).
[5]G. F. Miller and H. Pursey, "The field and radiation impedance of mechanical radiators on the free surface of a semi-infinite isotropic solid," Proc. R. Soc. London, Ser. A **223**, 521–541 (1954).
[6]G. F. Miller and H. Pursey, "On the partition of energy between elastic waves in a semi-infinite solid," Proc. R. Soc. London, Ser. A **223**, 55–69 (1955).
[7]C. R. Farrar, S. W. Doebling, and D. A. Nix, "Vibration-based structural damage identification," Philos. Trans. R. Soc. London **359**, 131–149 (2001).
[8]H. Tohmyoh, M. A. S. Akanda, "Sensitivity of acoustic microscopy for detecting three-dimensional nanometer gaps embedded in a silicon structure," J. Acoust. Soc. Am. **126**, 98–102 (2009).
[9]W. P. Rogers, "Elastic property measurement using Rayleigh–Lamb waves," Res. Nondestruct. Eval. **6**, 185–208 (1995).
[10]L. Gao, K. J. Parker, S. K. Alam, and R. M. Lerner, "Sonoelasticity imaging: Theory and experimental verification," J. Acoust. Soc. Am. **97**, 3875–3886 (1995).
[11]S. Catheline, F. Wu, and M. Fink, "A solution to diffraction biases in sonoelasticity: The acoustic impulse technique," J. Acoust. Soc. Am. **105**, 2941–2950 (1999).
[12]Y. Yamakoshi, J. Sato, and T. Sato, "Ultrasonic imaging of internal vibration of soft tissue under forced vibration," IEEE Trans. Ultrason. Ferroelectr. Freq. Control **37**, 45–53 (1990).
[13]R. Muthupillai, D. J. Lomas, P. J. Rossman, J. F. Greenleaf, A. Manduca, and R. L. Ehman, "Magnetic resonance elastography by direct visualization of propagating acoustic strain waves," Science **269**, 1854–1857 (1995).
[14]S. F. Othman, H. Xu, T. J. Royston, and R. L. Magin, "Microscopic magnetic resonance elastography (μMRE)," Magn. Reson. Med. **54**, 605–614 (2005).
[15]F. A. Duck, *Physical Properties of Tissue: A Comprehensive Reference Book* (Academic, New York, 1990).
[16]V. Kuperman, *Magnetic Resonance Imaging: Physical Principles and Applications* (Academic, New York, 2000).
[17]K. Hoyt, T. Kneezel, B. Castaneda, and K. J. Parker, "Quantitative sonoelastography for the in vivo assessment of skeletal muscle viscoelasticity," Phys. Med. Biol. **53**, 4063–4080 (2008).
[18]Y. C. Fung, *Biomechanics: Mechanical Properties of Living Tissues*, 2nd ed. (Springer-Verlag, New York, 1993).
[19]A. P. Sarvazyan, O. V. Rudenko, S. D. Swanson, J. B. Fowlkes, and S. Y. Emelianov, "Shear wave elasticity imaging: A new ultrasonic technology of medical diagnostics," Ultrasound Med. Biol. **24**, 1419–1435 (1998).
[20]R. Muthupillai, P. J. Rossman, D. J. Lomas, J. F. Greenleaf, S. J. Riederer, and R. L. Ehman, "Magnetic resonance imaging of transverse acoustic strain waves," Magn. Reson. Med. **36**, 266–274 (1996).
[21]T. E. Oliphant, A. Manduca, R. L. Ehman, and J. F. Greenleaf, "Complex-valued stiffness reconstruction for magnetic resonance elastography by algebraic inversion of the differential equation," Magn. Reson. Med. **45**, 299–310 (2001).
[22]A. J. Romano, J. J. Shirron, and J. A. Bucaro, "On the noninvasive determination of material parameters from a knowledge of elastic displacements: Theory and numerical simulation," IEEE Trans. Ultrason. Ferroelectr. Freq. Control **45**, 751–759 (1998).
[23]A. J. Romano, J. A. Bucaro, R. L. Ehman, and J. J. Shirron, "Evaluation of a material parameter extraction algorithm using MRI-based displacement measurements," IEEE Trans. Ultrason. Ferroelectr. Freq. Control **47**, 1575–1581 (2000).
[24]E. E. Van Houten, M. M. Doyley, F. E. Kennedy, J. B. Weaver, and K. D. Paulsen, "Initial in vivo experience with steady-state subzone-based MR Elastography of the human breast," J. Magn. Reson Imaging **17**, 72–85 (2003).
[25]E. E. Van Houten, M. M. Doyley, F. E. Kennedy, K. D. Paulsen, and J. B. Weaver, "A three-parameter mechanical property reconstruction method for MR-based elastic property imaging," IEEE Trans. Med. Imaging **24**, 311–324 (2005).
[26]S. G. Chen, M. Fatemi, and J. F. Greenleaf, "Remote measurement of material properties from radiation force induced vibration of an embedded sphere," J. Acoust. Soc. Am. **112**, 884–889 (2002).
[27]S. G. Chen, M. Fatemi, and J. F. Greenleaf, "Quantifying elasticity and viscosity from measurement of shear wave speed dispersion," J. Acoust. Soc. Am. **115**, 2781–2785 (2004).
[28]S. G. Chen, M. Fatemi, and J. F. Greenleaf, "Shearwave dispersion ultrasound vibrometry (SDUV) for measuring tissue elasticity and viscosity," IEEE Trans. Ultrason. Ferroelectr. Freq. Control **56**, 55–62 (2009).
[29]R. W. Chan and I. R. Titze, "Effect of postmortem changes and freezing on the viscoelastic properties of vocal fold tissues," Ann. Biomed. Eng. **31**, 482–491 (2003).
[30]D. Craiem and R. Armentano, "A fractional derivative model to describe arterial viscoelasticity," Biorheology **44**, 251–263 (2007).
[31]M. Z. Kiss, T. Varghese, and T. J. Hall, "Viscoelastic characterization of *in vitro* canine tissue," Phys. Med. Biol. **49**, 4207–4218 (2004).
[32]D. Klatt, U. Hamhaber, P. Asbach, J. Braun, and I. Sack, "Noninvasive assessment of the rheological behavior of human organs using multifrequency MR elastography: A study of brain and liver viscoelasticity," Phys. Med. Biol. **52**, 7281–7294 (2007).
[33]R. Sinkus, K. Siegmann, T. Xydeas, M. Tanter, C. Claussen, and M. Fink, "MR Elastography of breast lesions: Understanding the solid/liquid duality can improve the specificity of contrast-enhanced MR mammography," Magn. Reson. Med. **58**, 1135–1144 (2007).
[34]T. J. Royston, H. A. Mansy, and R. H. Sandler, "Excitation and propagation of surface waves on a viscoelastic half-space with application to medical diagnosis," J. Acoust. Soc. Am. **106**, 3678–3686 (1999).
[35]T. J. Royston, Y. Yazicioglu, and F. Loth, "Surface response of a viscoelastic medium to subsurface acoustic sources with application to medical diagnosis," J. Acoust. Soc. Am. **113**, 1109–1121 (2003).
[36]H. L. Oestreicher, "Field and impedance of an oscillating sphere in a viscoelastic medium with an application to biophysics," J. Acoust. Soc. Am. **23**, 707–714 (1951).
[37]R. L. Magin, *Fractional Calculus in Bioengineering* (Begell House, Redding, CT, 2006).
[38]S. P. Timoshenko and J. N. Goodier, *Theory of Elasticity*, 3rd ed. (McGraw-Hill, New York, 1970).
[39]C. L. Pekeris, "The seismic surface pulse," Proc. Natl. Acad. Sci. U.S.A. **41**, 469–480 (1955).